

Actively tunable dual-broadband graphene-based terahertz metamaterial absorber

Dan Hu(胡丹), Tian-Hua Meng(孟田华), Hong-Yan Wang(王红燕), and Mai-Xia Fu(付麦霞)

Citation: Chin. Phys. B, 2021, 30 (**12**): 126101. DOI: 10.1088/1674-1056/ac0794
Journal homepage: http://cpb.iphy.ac.cn; http://iopscience.iop.org/cpb

What follows is a list of articles you may be interested in

Highly tunable plasmon-induced transparency with Dirac semimetal metamaterials

Chunzhen Fan(范春珍), Peiwen Ren(任佩雯), Yuanlin Jia(贾渊琳), Shuangmei Zhu(朱双美), and Junqiao Wang(王俊俏)

Chin. Phys. B, 2021, 30 (**9**): 096103. DOI: 10.1088/1674-1056/abf4bf

Electronic structure of single-crystalline graphene grown on Cu/Ni (111) alloy film

Xue-Fu Zhang(张学富), Zhong-Hao Liu(刘中灏), Wan-Ling Liu(刘万领), Xiang-Le Lu(卢祥乐), Zhuo-Jun Li(李卓君), Qing-Kai Yu(于庆凯), Da-Wei Shen(沈大伟), Xiao-Ming Xie(谢晓明)

Chin. Phys. B, 2019, 28 (**8**): 086103. DOI: 10.1088/1674-1056/28/8/086103

Realization of THz dualband absorber with periodic cross-shaped graphene metamaterials

Chunzhen Fan(范春珍), Yuchen Tian(田雨宸), Peiwen Ren(任佩雯), Wei Jia(贾微)

Chin. Phys. B, 2019, 28 (**7**): 076105. DOI: 10.1088/1674-1056/28/7/076105

Low-temperature growth of large-scale, single-crystalline graphene on Ir(111)

Hui Guo(郭辉), Hui Chen(陈辉), Yande Que(阙炎德), Qi Zheng(郑琦), Yu-Yang Zhang(张余洋), Li-Hong Bao(鲍丽宏), Li Huang(黄立), Ye-Liang Wang(王业亮), Shi-Xuan Du(杜世萱), Hong-Jun Gao(高鸿钧)

Chin. Phys. B, 2019, 28 (**5**): 056107. DOI: 10.1088/1674-1056/28/5/056107

Dynamically tunable optical properties in graphene-based plasmon-induced transparency metamaterials

Wei Jia(贾微), Pei-Wen Ren(任佩雯), Yu-Chen Tian(田雨宸), Chun-Zhen Fan(范春珍)

Chin. Phys. B, 2019, 28 (**2**): 026102. DOI: 10.1088/1674-1056/28/2/026102

Actively tunable dual-broadband graphene-based terahertz metamaterial absorber*

Dan Hu(胡丹)[1,†], Tian-Hua Meng(孟田华)[2], Hong-Yan Wang(王红燕)[3], and Mai-Xia Fu(付麦霞)[4]

[1] School of Physics and Electrical Engineering, Anyang Normal University, Anyang 455000, China
[2] Department of Physics and Electronics Science, Shanxi Datong University, Datong 037009, China
[3] School of Education Information Technology and Communication, Anyang Normal University, Anyang 455000, China
[4] College of Information Science and Engineering, Henan University of Technology, Key Laboratory of Grain Information Processing and Control, Ministry of Education, Zhengzhou 450001, China

(Received 1 March 2021; revised manuscript received 29 April 2021; accepted manuscript online 3 June 2021)

A tunable metamaterial absorber (MA) with dual-broadband and high absorption properties at terahertz (THz) frequencies is designed in this work. The MA consists of a periodic array of flower-like monolayer graphene patterns at top, a SiO_2 dielectric spacer in middle, and a gold ground plane at the bottom. The simulation results demonstrate that the designed MA has two wide absorption bands with an absorption of over 90% in frequency ranges of 0.68 THz–1.63 THz and 3.34 THz–4.08 THz, and the corresponding relative bandwidths reach 82.3% and 20%, respectively. The peak absorptivity of the absorber can be dynamically controlled from less than 10% to nearly 100% by adjusting the graphene chemical potential from 0 eV to 0.9 eV. Furthermore, the designed absorber is polarization-insensitive and has good robustness to incident angles. Such a high-performance MA has broad application prospects in THz imaging, modulating, filtering, *etc.*

Keywords: metamaterial, graphene, absorber, terahertz

PACS: 61.48.Gh, 42.50.Gy, 42.25.Bs, 78.67.Pt **DOI:** 10.1088/1674-1056/ac0794

1. Introduction

Metamaterials are comprised of periodically or non-periodically arranged artificial subwavelength structures and exhibit the remarkable physical properties not observed in nature, such as high refractive index and negative refractive index.[1,2] These properties have been utilized to achieve some new functions, like superlensing,[3,4] invisibility cloaking,[5,6] and perfect absorption.[7,8] In recent years, more and more attention has been paid to metamaterial-based perfect absorbers since they not only possess the advantages of high absorption, design flexibility, and thin thickness, but also have promising application prospects in thermal emitters,[9] sensors,[10,11] stealth technology,[12] and images.[13] Since Landy *et al.* first proposed and experimentally demonstrated a perfect microwave MA composed of a metal split-ring resonator and a metal wire separated by a dielectric spacer,[14] various kinds of MAs have been proposed to obtain single-band, dual-band, multiband, and broadband perfect light absorptions, and their working frequency ranges have been moved from initial microwave to infrared, THz, and visible regions.[7–16] However, these MAs are constructed mainly by using metallic metamaterial structures; consequently, their absorption properties are difficult to tune, which leads to a lack of flexibility.

Graphene, as a new kind of two-dimensional (2D) nanomaterial composed of a monolayer carbon atom densely arranged in a honeycomb crystal lattice,[17] is considered to be the one of the most promising materials due to its unique and intriguing physical properties. For instance, the electrical conductivity of graphene can be dynamically tuned by adjusting its chemical potential via external gate voltage or chemical doping.[18,19] Recently, many tunable MAs with structured and nonstructured graphene have been presented.[20–27] However, most of them still exhibit narrow absorption bandwidth, which greatly hinders their practical applications in some fields, such as stealth technology. To increase the absorption bandwidth, several design approaches have been proposed, including coplanar multiple structured graphene patterns in one-unit cell,[28–33] stacked multilayer graphene patterns,[34–40] and hybrid graphene–metal or dielectric patterns.[41–50] Although these approaches can solve the above problems, they still have some shortcomings, such as complicated fabrication processes, complex structures.

In this work, we present a tunable dual-broadband metamaterial absorber based on a simple monolayer graphene pattern in the THz region. Compared with the above-mentioned graphene-based broadband MAs, our proposed MA possesses the characteristics of dual-band, broadband, and simple geometric structure besides the polarization-insensitive and wide-angle high absorption. The simulated results indicate that the proposed MA has two wide absorption bands, *i.e.*, 0.68 THz–

*Project supported by the National Natural Science Foundation of China (Grant Nos. 11504006 and 61805072) and the Key Scientific Research Project of Colleges and Universities in Henan Province, China (Grant No. 22A140001).

†Corresponding author. E-mail: tylzhd@163.com

© 2021 Chinese Physical Society and IOP Publishing Ltd

1.63 THz and 3.34 THz–4.08 THz in which bands both absorptions reach over 90%, and the corresponding relative bandwidths are 82.3% and 20%, respectively. Additionally, the peak absorptivity of the proposed MA can be changed by tuning the chemical potential of graphene. The impedance matching theory is employed to understand the physical origin of the proposed MA. The electrical field, magnetic field, and surface current distributions are also presented to further understand the physical origin of this absorber. Finally, the influences of geometric parameters and incident angles on its absorption performance are also studied. Our results may provide an alternative way to achieve dual-broadband tunable metamaterial devices in THz or other frequency ranges.

2. Methods

Figure 1 displays a schematic diagram of one unit cell of the array of the proposed MA, which consists of a single-layer flower-like graphene pattern and an ultra-thin metallic ground film, separated by a loss-free SiO_2 dielectric layer with a thickness of $t = 32$ μm and a relative permittivity of $\varepsilon = 3.9$.[29] The flower-like graphene pattern is composed of four identical elliptical disks, which is also a 45° rotating cross-like. The major axis length of the elliptical disk is $l = 19.5$ μm, and the minor axis length is $m = 9.25$ μm. The period of the unit cell is $p = 30$ μm. The bottom metallic plane is of gold, and has a thickness of $d = 0.5$ μm and an electrical conductivity of $\sigma = 4.09 \times 10^7$ S/m.[29] The surface conductivity (σ_g) of graphene can be gained from the well-known Kubo formula[51]

$$\sigma_g(\omega) = \frac{ie^2 k_B T}{\pi\hbar(\omega + i\tau^{-1})}\left[\frac{\mu_c}{k_B T} + 2\ln(e^{-\mu_c/k_B T} + 1)\right] + \frac{ie^2}{4\pi\hbar}\ln\left[\frac{2|\mu_c| - \hbar(\omega + i\tau^{-1})}{2|\mu_c| + \hbar(\omega + i\tau^{-1})}\right], \quad (1)$$

where e is the electron charge, T is the temperature, ω is the radian frequency, and τ is the electron–phonon relaxation time. And k_B, $\hbar$, and μ_c are the Boltzmann constant, the reduced Planck constant ($\hbar = h/2\pi$), and the chemical potential, respectively. According to Eq. (1), the surface conductivity (σ_g) of graphene can be tuned by changing the chemical potential μ_c. And the chemical potential μ_c can be dynamically controlled by the ion-gel top gating method[52] as shown in Fig. 1(b).

The optical properties of the proposed MA are investigated numerically by using the frequency domain solver in CST Microwave Studio, where the unit cell boundary condition is arranged in the x and y directions of the unit cell under the open boundary condition in the z direction. The single-layer graphene sheet is modelled as an equivalent 2D surface impedance layer with $Z_g = 1/\sigma_g$ and zero thickness.[30,31] Throughout this paper, the temperature (T) and the electron–phonon relaxation time (τ) are set to be 300 K and 0.13 ps, respectively. The chemical potential (μ_c) is initially assumed to be 0.9 eV. The absorption $A(\omega)$ of the proposed MA is calculated from $A(\omega) = 1 - R(\omega) - T(\omega)$, where $R(\omega) = |S_{11}(\omega)|^2$ and $T(\omega) = |S_{21}(\omega)|^2$ are the reflection and transmission, respectively, $S_{11}(\omega)$ and $S_{21}(\omega)$ are the frequency-dependent S-parameters, which can be obtained by the CST Microwave Studio simulation. The transmission $T(\omega)$ can be ignored since the gold ground film is so thick that it interrupts the transmitted THz wave. In practice, a single-layer and larger-area graphene film can be grown by using an optimized liquid-precursor chemical vapor deposition method, and the flower-like pattern can be fabricated by electron beam lithography and oxygen plasma etching.[52]

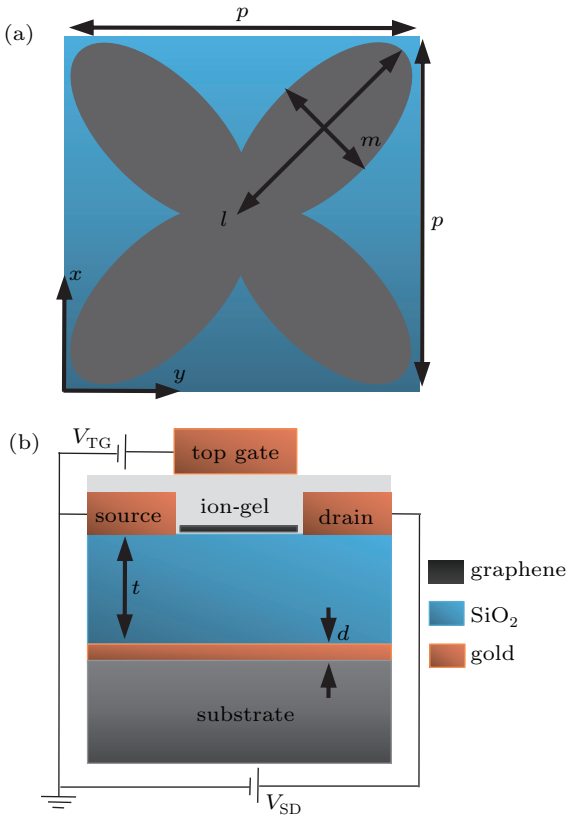


Fig. 1. Schematic diagram of (a) unit cell of proposed MA and (b) top-gate structure tuning graphene chemical potential.

3. Results and discussion

The calculated absorption, transmission and reflection spectra of the proposed MA under normal incidence for both TE (the electric field is parallel to the x axis) mode and TM (the electric field is parallel to the y axis) mode as displayed in Fig. 2(a). The transmission is nearly zero. The absorption spectra for TE mode and TM mode are the same. It is clear that the proposed MA has four perfect absorption peaks at 0.80 (f_1), 1.47 (f_2), 3.58 (f_3), and 3.87 THz (f_4) with absorption rates of 98.68%, 96.51%, 97.78%, and 97.94%, re-

spectively. The four absorption peaks together construct two broad absorption bands. The relative bandwidths of the two bands over 90% absorption rate are about 82.3% and 20% in the frequency ranges of 0.68 THz–1.63 THz and 3.34 THz–4.08 THz with central frequencies of 1.155 THz and 3.71 THz, respectively.[32] Figure 2(b) shows the color map of the absorption spectra with the polarization angle φ increasing 0° to 90°. It can be seen that the proposed MA possesses an excellent polarization-independent property due to the fourfold rotational symmetry of the designed structure.

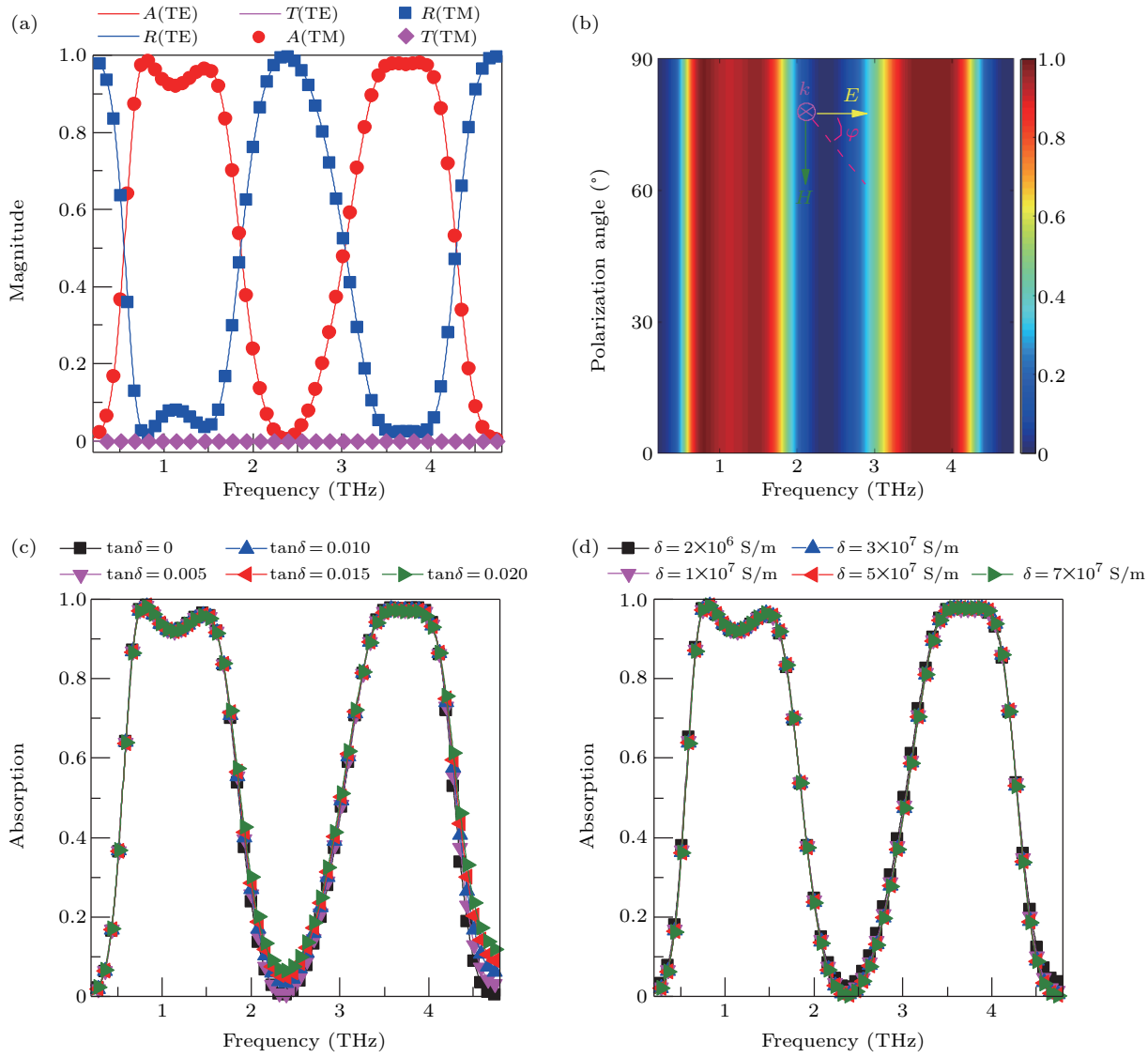


Fig. 2. (a) Transmission, reflection, and absorption spectra of proposed MA. (b) Absorption of proposed MA *versus* frequency and polarization angle φ. Absorption spectra of proposed MA with different losses from (c) dielectric spacer and (d) metallic ground plan.

Next, we investigate the influences of the loss from the dielectric spacer and the metallic ground plane on the absorption spectra of the proposed MA. As shown in Fig. 2(c), we can see that when increasing the dielectric loss tangent ($\tan\delta$) from 0 to 0.02, the absorption spectra remain almost unchanged. The magnitude change of the electrical conductivity from the metallic ground plane also does not influence the absorption spectra, as shown in Fig. 2(d). These results indicate that the energy of incident THz radiation is almost dissipated in the structured graphene layer, and thus having more choices for dielectric and metal materials.

The physical mechanism of the dual-broadband perfect absorption can be interpreted by the impedance matching theory. According to the impedance matching theory, the effective impedance (Z) of the proposed MA can be calculated by the expression[53]

$$Z = \sqrt{\frac{(1+S_{11}(\omega))^2 - S_{21}(\omega)^2}{(1+S_{11}(\omega))^2 + S_{21}(\omega)^2}}, \tag{2}$$

where $S_{11}(\omega)$ and $S_{21}(\omega)$ are respectively the complex-amplitude reflection and transmission coefficients when THz wave is normally incident on the proposed MA. Figure 3 shows the real part and imaginary part of the effective impedance Z. It is obvious that the real part is close to 1 and the imaginary part approaches to zero in the frequency ranges of 0.68 THz–1.63 THz and 3.34 THz–4.08 THz. It means that

the impedance between the proposed MA and the free space nearly matches with each other. Therefore, a dual-broadband absorber with high absorption is achieved due to the low reflection and nearly zero transmission of the proposed MA in these two frequency ranges.

To gain an insight into the physical origin of the dual-broadband absorption, the electric field ($|E|$) distributions on the x–y plane at four near-perfect absorption peaks for TE mode are plotted in Figs. 4(a)–4(d). For modes f_1 and f_2, the strong electric fields are assembled mainly at the upper end and lower end of the graphene pattern (along the x-axis direction): a small fraction on the left side and right side of the graphene pattern (see Figs. 4(a) and 4(b)). In contrast, the strong electric fields in modes f_3 and f_4 are concentrated mainly on the edges except for the ends of the graphene pattern (see Figs. 4(c) and 4(d)). The total absorption of the electromagnetic energy inside graphene can be evaluated by the following equation:

$$A(\omega) = \omega\varepsilon'' \int_S |E|^2 \mathrm{d}S, \tag{3}$$

where ω is the angular frequency, ε'' is the imaginary part of the graphene permittivity, E is the electric field inside graphene, and S is the surface area of the graphene.[39] According to Eq. (3), one can see that the electromagnetic energy loss is mainly dissipated in the graphene layer, further implying that the proposed graphene structure plays an important role in enhancing absorption.

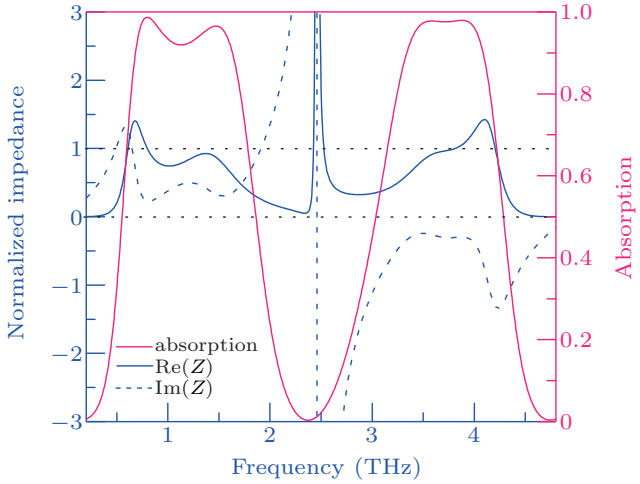


Fig. 3. Curves of effective impedance (Z) of proposed MA, with blue solid line and blue dash line representing Re (Z) and Im (Z), respectively, and red dash line referring to absorption spectrum which is presented for contrast.

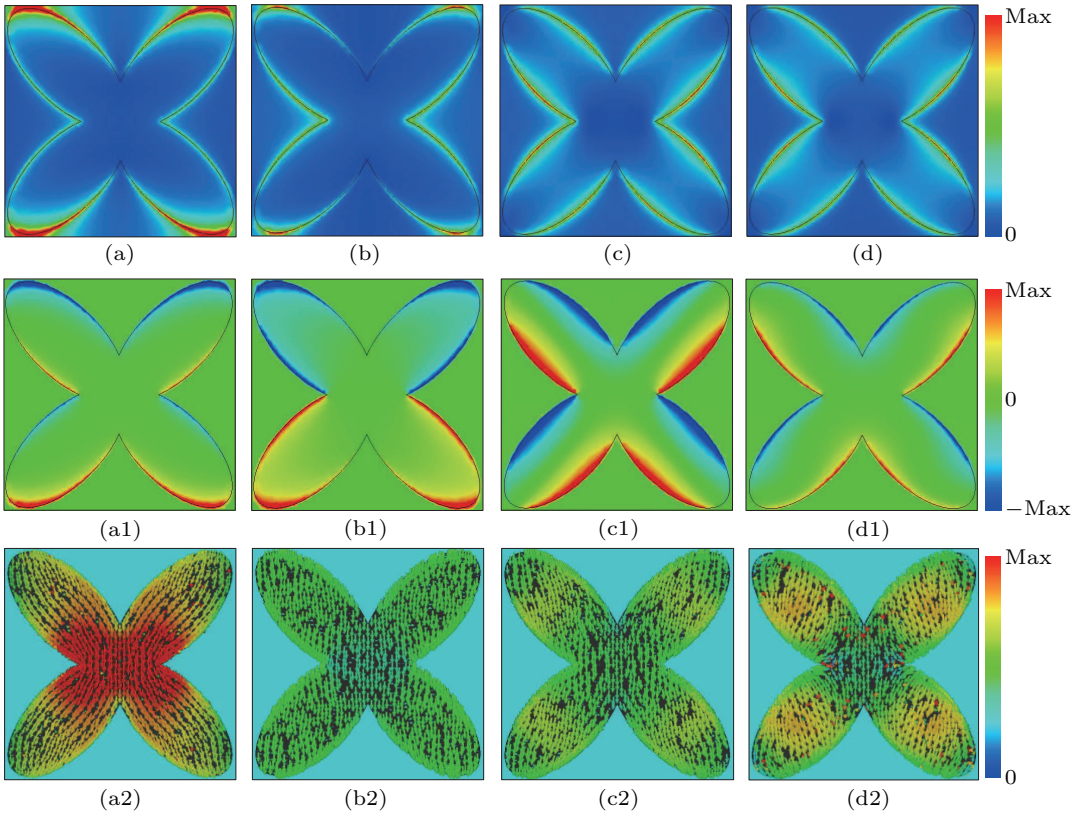


Fig. 4. Distributions of [(a)–(d)] electric field ($|E|$), [(a1)–(d1)] z-component electric field (E_z), and [(a2)–(d2)] surface current for proposed MA at absorption peak frequencies of [(a)–(a2)] 0.80 THz, [(b)–(b2)] 1.47 THz , [(c)–(c2)] 3.58 THz, and [(d)–(d2)] 3.87 THz, respectively.

Furthermore, the z-component electric field (E_z) and surface current distributions at these absorption peak frequencies are provided as shown in Figs. 4(a1)–4(d1) and 4(a2)–4(d2), respectively. The distribution of E_z in mode f_1 is similar to that of $|E|$ in Fig. 4(a). Opposite charges gather mainly on the upper and lower end of the graphene pattern (see Fig. 4(a1)), indicating excitation of loop current in the surface of the graphene pattern. It can be seen from Fig. 4(a2)

that the surface current flows from upper end to lower end along the major axis direction of the elliptical disk. Thus, this kind of resonance mode is attributed to *LC* resonance of the graphene pattern. Unlike the mode f_1, the opposite charges in mode f_2 concentrate mainly on the upper and lower half of the graphene pattern (see Fig. 4(b1)). The surface current flows from upper elliptical disk to lower one on the same side of the graphene pattern (see Figs. 4(b2)). It indicates that the mode f_2 is due to dipole resonance of the graphene pattern. For mode f_3, its E_z distribution is also similar to that of $|E|$ in Fig. 4(c1). The surface charges are accumulated on the edges except for the ends of the graphene pattern. Thus, this kind of resonance mode also originates from dipole response of the graphene pattern. Similarly, for mode f_4, its E_z (see Fig. 4(d1)) is also similar to that of the mode f_3 in Fig. 4(c1). Thus, mode f_4 is also attributed to the dipole response of the graphene pattern. From Figs. 4(c2) and 4(d2), it can be seen that the surface current flows along the major-axis direction of elliptical disk for mode f_3, but it flows along the minor-axis direction for mode f_4. It means that the effective length of mode f_3 is larger than that of mode f_4, so the resonance frequency of mode f_3 is lower than that of mode f_4.

Additionally, from the magnetic field distributions of the y–z plane ($x = 0$) at the four absorption peak frequencies, the physical mechanism of the dual-broadband absorption can be understood as shown in Fig. 5. From Figs. 5(a)–5(d), one sees that the magnetic field is distributed in the loss-free SiO_2 dielectric layer. The magnetic field distribution strongly attests to the existence of the magnetic dipole.[54] Also, one can see from Fig. 5(a) that strong magnetic field assembles on the left gap and the right gap of the graphene pattern, which further confirms that the mode f_1 is due to the *LC* resonance.[55] From the above analysis, we can see that the combination of *LC*, dipole, and magnetic responses can produce dual-broadband perfect absorption. Although the conclusion is discussed under TE mode, a similar situation appears at TM mode and the physical origin of dual-broadband absorption is precisely the same.

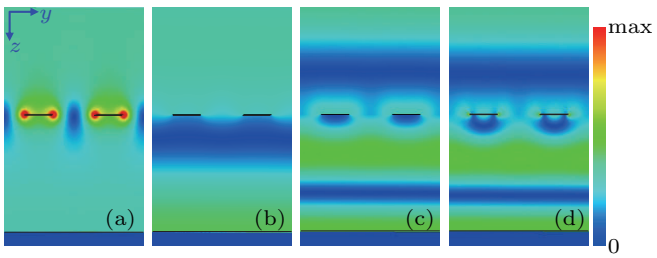


Fig. 5. Distributions of magnetic field on y–z plane ($x = 0$) for proposed MA at absorption peak frequencies of (a) 0.80 THz, (b) 1.47 THz, (c) 3.58 THz, and (d) 3.87 THz respectively.

To further understand the physical origin of the proposed MA, we discuss the influence of geometric parameters on absorption spectra. Figures 6(a) and 6(b) show the absorption spectra of the proposed MA with different lengths of major axis (l) and minor axis (m) of the elliptical graphene disk, respectively. As shown in Fig. 6(a), as l increases from 15.5 μm to 19.5 μm, the resonance frequencies of the first absorption band decrease to different degrees and the absorptivity of the first absorption band is also sensitive to the change of the l, while the frequency and absorption of the second absorption band have only a slight change, for which the reason is that the electric field of the first absorption band is more sensitive to the l than that of the second absorption band. For minor axis length m varying from 9.25 μm to 6.25 μm, it can be found from Fig. 6(b) that the resonance frequency of the first absorption band has an opposite change trend with the decrease of m, while the absorptivity of the first absorption band is insensitive to the change of m. However, for the second absorption band, the absorptivity decreases sharply, and it becomes a narrow absorption band since the mode f_4 gradually disappears with the decrease of m, fow which the reason is that the electric fields of the second absorption band accumulate mainly on the both sides of the elliptical graphene disk (along the minor axis direction); its absorption is sensitive to the change of m. Figure 6(c) shows the influence of period (p) on the absorption spectrum. It can be seen from Fig. 6(c) that when the p increases from 30 μm to 38 μm, the bandwidths of the two absorption bands decrease but the peak absorptivities increase. That is because the changes of the p can influence the interaction with adjacent cells. From Fig. 6(d), it is found that when the thickness of dielectric layer (t) increases from 30 μm to 34 μm, the two absorption bands are red-shifted and the peak absorptivities change to different degrees since the change of the t influences the relative impedance of the absorber. And it indicates that the t designed as 32 μm is better to achieve broadband high absorption performance for the whole structure. These results demonstrate that the geometric parameters of the proposed graphene structure directly determine the frequency and absorptivity of the proposed MA to a certain extent. However, the two broad absorption bands always remain over 90% as the geometric parameters are varied in a certain range. According to the discussion above, we can conclude that our dual-broadband absorber has high fabrication tolerance.

The effect of chemical potential μ_c on absorption spectra is shown in Fig. 7. When the chemical potential (μ_c) increases from 0 eV to 0.9 eV, the peak absorptivity can be turned from 27.78% to nearly 100% for the first absorption band, and from 7.67% to nearly 100% for the second absorption band. Furthermore, the tunable absorption characteristics of the proposed MA are the same under the TE mode and TM mode. Therefore, the proposed MA has broad application prospects in dynamic modulators, switchers and other THz components.

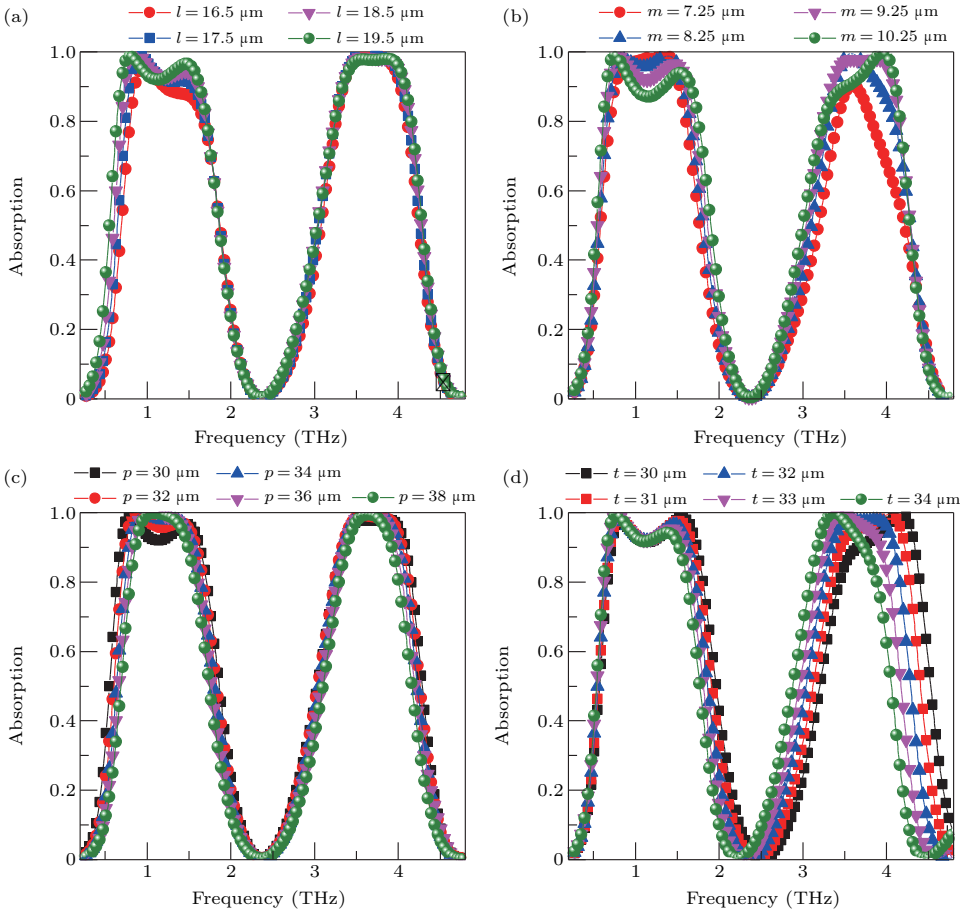


Fig. 6. Dependence of absorption spectra of proposed MA on (a) major axis length l , (b) minor axis length m of the elliptical graphene disk, (c) period p, and (d) thickness of SiO_2 dielectric layer t.

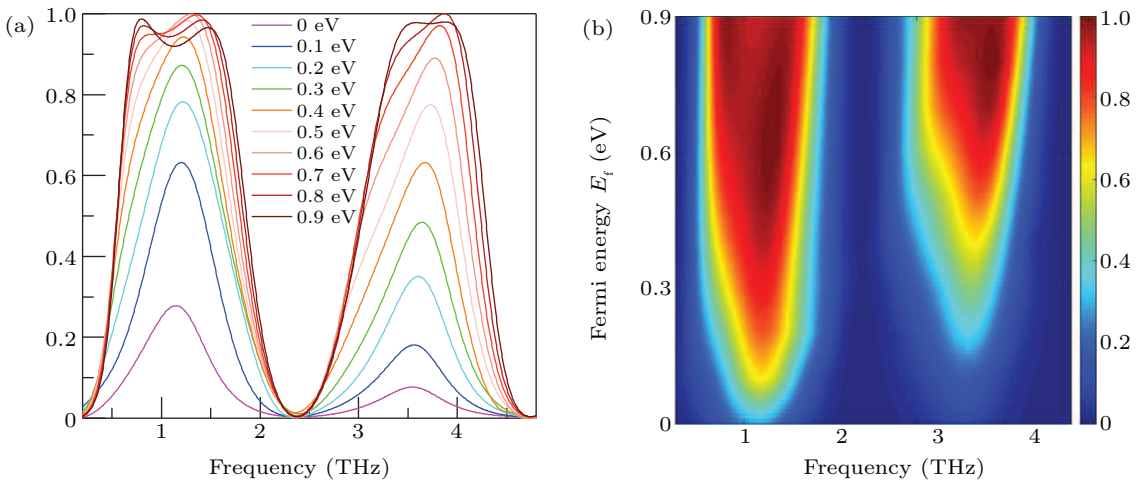


Fig. 7. Absorption spectra and colormap with chemical potential ranging from 0 eV to 0.9 eV for (a) TE mode and TM (b) mode under normal incidence, respectively.

The wide-angle characteristic is very important for practical applications of absorbers, and the absorption should be as robust as possible over a wide range of incident angles. To investigate the angle dependence of the absorber, the dependence of the absorption spectra on the incident angle (θ) for TE mode and TM mode are shown in Fig. 8. It is clear that the absorber shows a prominent absorption performance with relatively stable absorption and bandwidth over a wide range of incident angle for the TE mode and the TM mode. For the first absorption band, the absorption is over 80% in a frequency range of 0.71 THz–1.70 THz even at 40° for TE mode and at 60° for TM mode, respectively. For the second absorption band, the absorption remains over 80% in a frequency range of 3.48 THz–4.16 THz until the incident angle increases up to 40° for TE mode and to 50° for TM mode. It implies that the proposed MA shows a good absorption performance with

a wide incident angles for the TE mode and the TM mode.

Now, we come to evaluate the performance of the proposed MA and compare it with other recent published broadband THz absorbers (see Table 1). Compared with the given graphene-based broadband MAs, our presented MA has at least two merits: one of them is that our absorber is not only simple in design, but also avoids some disadvantages, such as large unit size, complicated geometric structure and fabrication process, and the other is that the relative bandwidth of the first absorption band is 82.3% with an absorption over 90%, which is even larger than those with single broadband structures[29,31,33,37,39,42,44] and dual broadband structure.[56] Comparing with the second absorption band of the dual-broadband graphene-based MA,[43,56] our proposed structure also exhibits good absorption performance including relative absorption bandwidth (over 90% absorption) and peak absorption rate. Compared with the broadband THz absorbers based on vertically aligned carbon nanotubes and 3D MXene,[57,58] our absorber has a relative narrow bandwidth, but it has an ultrathin thickness which is conducive to the development of miniaturized and integrated THz devices.

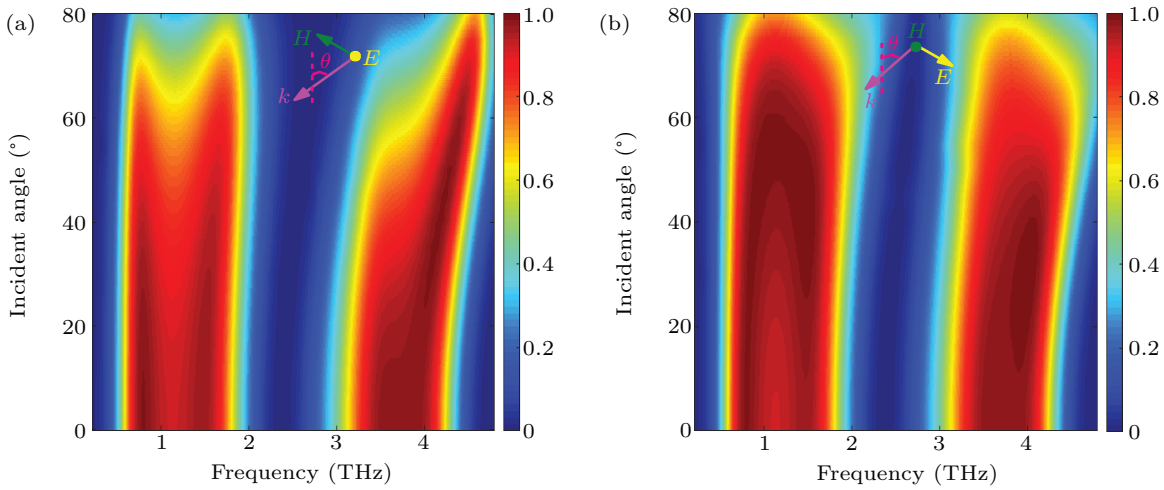


Fig. 8. Absorption of proposed MA with incident angle θ ranging from 0° to 80° for (a) TE mode and (b) TM modes ($\mu_c = 0.9$ eV).

Table 1. Comparison of proposed absorber with published broadband THz absorbers..

References	Type	Absorption (%)	Relative bandwidth (%)	Structure
[28]	broad	≥ 90	84.5	coplanar multiple substructures
[29]	broad	≥ 90	33.3	coplanar multiple substructures
[30]	broad	≥ 90	90.5	coplanar multiple substructures
[31]	broad	≥ 90	81.44	coplanar multiple substructures
[32]	broad	≥ 90	90.32	coplanar multiple substructures
[33]	broad	≥ 90	79.2	coplanar multiple substructures
[34]	broad	≥ 90	84.6	multi-layer structures
[35]	broad	≥ 90	140	multi-layer structures
[37]	broad	≥ 90	25.4	multi-layer structures
[38]	broad	≥ 90	88.88	multi-layer structures
[39]	broad	≥ 90	12.4	multi-layer structures
[42]	broad	≥ 90	65.8	hybrid graphene-metal structure
[43]	dual broad	≥ 80	97.8, 31	hybrid graphene-dielectric structure
[44]	broad	≥ 90	66.7	hybrid graphene-metal structure
[45]	broad	≥ 90	61	hybrid graphenesemimetal structure
[56]	dual broad	≥ 95	31.2, 10.5	an asymmetric structure
[57]	broad	≥ 90	187.1	vertically aligned carbon nanotubes
[58]	broad	≥ 90	163.63	3D MXene/GO foam
This work	dual broad	≥ 90	82.3, 20	a symmetric structure

4. Conclusion

In this work, a simple graphene pattern is proposed to realize a tunable THz MA with dual-broadband and high absorption. It consists of a flower-like graphene pattern array and a gold ground plane separated by a thin SiO_2 dielectric spacer. Simulation results show that the two relative bandwidths with over 90% absorption are 82.3% and 20% in the frequency ranges of 0.68 THz–1.63 THz and 3.34 THz–4.08 THz, respectively. By modifying the chemical potential of graphene, the peak absorptivity can be turned from 27.78% to nearly

100% for the first absorption band, and from 7.67% to nearly 100% for the second absorption band. Furthermore, the proposed MA is insensitive to polarization angle and maintains stable absorption performance well for the TE mode and the TM mode over a wide range of incident angles. The proposed MA may serve as a potential candidate in THz modulators and detectors, *etc.*

References

[1] Choi M, Lee S H, Kim Y, Kang S B, Shin J, Kwak M H, Kang K Y, Lee Y H, Park N and Min B 2011 *Nature* **470** 369
[2] Ozbay E, Guven K and Aydin K 2007 *J. Opt. A: Pure Appl. Opt.* **9** S301
[3] Zhang X and Liu Z W 2008 *Nat. Mater.* **7** 435
[4] Fang N, Lee H, Sun C and Zhang X 2005 *Science* **308** 534
[5] Ergin T, Stenger N, Brenner P, Pendry J B and Wegener M 2010 *Science* **328** 337
[6] Alitalo P and Tretyakova S 2009 *Mater. Today* **12** 22
[7] Hu D, Wang H Y and Zhu Q F 2016 *IEEE Photon. J.* **8** 5500608
[8] Watts C M, Liu X L and Padilla W J 2012 *Adv. Mater.* **24** OP98
[9] Diem M, Koschny T, Soukoulis C M 2009 *Phys. Rev. B* **79** 033101
[10] Grant J, Carranza I E, Li C, McCrindle I J H, Gough J and Cumming D R S 2013 *Laser Photon. Rev.* **7** 1043
[11] Liu N, Mesch M, Weiss T and Hentschel M 2010 *Nano Lett.* **10** 2342
[12] Kim J, Han K and Hahn J W 2017 *Sci. Rep.* **7** 6740
[13] Fan K B, Suen J Y, Liu X Y and Padilla W J 2017 *Optica* **4** 601
[14] Landy N I, Sajuyigbe S, Mock J J, Smith D R and Padilla W J 2008 *Phys. Rev. Lett.* **100** 207402
[15] Hu D, Wang H Y, Zhang X W, Wang K X and Zhu Q F 2019 *Sci. China-Inf. Sci.* **62** 069408
[16] Akselrod G M, Huang J N, Hoang T B, Bowen P T, Su L G, Smith D R and Mikkelsen M H 2015 *Adv. Mater.* **27** 8028
[17] Novoselov K S, Geiml A K, Morozov S V, Jiang D, Zhang Y, Dubonos S V, Grigorieva I V and Firsov A A 2004 *Science* **306** 666
[18] Grigorenko A, Polini M and Novoselov K 2012 *Nat. Photon.* **6** 749
[19] Mak K F, Ju L, Wang F and Heinz T F 2012 *Solid State Commun.* **152** 1341
[20] Alaee R, Farhat M, Rockstuhl C and Lederer F 2012 *Opt. Express* **20** 28017
[21] Xing R and Jian S S 2018 *Opt. Laser Technol.* **100** 129
[22] Zhang J G, Tian J P and Li L 2018 *IEEE Photon. J.* **10** 4800512
[23] Su Z P, Wang Y K, Luo X, Luo H, Zhang C, Li M X, Sang T and Yang G F 2018 *Phys. Chem. Chem. Phys.* **20** 14357
[24] Yao G, Ling F R, Yue J, Luo C Y, Ji J and Yao J Q 2016 *Opt. Express* **24** 1518
[25] Lin H, Ye X, Chen X F, Zhou Z G, Yi Z, Niu G, Yi Y G, Hua Y T, Hua J J and Xiao S Y 2019 *Mater. Res. Express* **6** 045807
[26] Ke S L, Wang B, Huang H, Long H, Wang K and Lu P X 2015 *Opt. Express* **23** 8888
[27] Barzegar-Parizi S, Ebrahimi A and Ghorbani K 2020 *Opt. Laser Technol.* **132** 106483
[28] Ye L F, Chen X, Cai G X, Zhu J F, Liu N and Liu Q H 2018 *Nanomaterials* **8** 562
[29] Mou NL, Sun SL, Dong HX, Dong SH, He Q, Zhou L and Zhang L 2018 *Opt. Express* **26** 11728
[30] Huang X, He W, Yang F, Ran J, Gao B and Zhang W L 2018 *Opt. Express* **26** 25558
[31] Li Y, Wu J, Wang C, Shen Z, Wu D, Wu N and Yang H 2019 *Phys. Scr.* **94** 035703
[32] Wu S, Zha D, Miao L, He Y and Jiang J 2019 *Phys. Scr.* **94** 105507
[33] Du X, Yan F, Wang W, Tan S, Zhang L, Bai Z, Zhou H and Hou Y 2020 *Opt. Laser Technol.* **132** 106513
[34] Amin M, Farhat M and Bağcı 2013 *Opt. Express* **21** 29938
[35] Rahmanzadeh M, Rajabalipanah H and Abdolali A 2018 *Appl. Opt.* **57** 959
[36] Daraeia O M, Goudarzi K and Bemani M 2020 *Opt. Laser Technol.* **122** 105853
[37] Fu P, Liu F, Ren G J, Su F, Li D and Yao J Q 2018 *Opt. Commun.* **417** 62
[38] Xu Z H, Wu D, Liu Y M, Liu C, Yu Z Y, Yu L and Ye H 2018 *Nanoscale Res. Lett.* **13** 143
[39] Cai Y J and Xu K D 2018 *Opt. Express* **26** 31693
[40] Cai Y J, Xu K D, Feng N X, Guo R R, Lin H J and Zhu J F 2019 *Opt. Express* **27** 3101
[41] Guo Y B, Wang S Q, Zhou Y G, Chen C Y, Zhu J F, Wang R and Cai Y J 2019 *J. Appl. Phys.* **126** 213103
[42] Zhao Y T, Wu B, Huang B J and Cheng Q 2017 *Opt. Express* **25** 7161
[43] Qi L M, Liu C and Shah S M A 2019 *Carbon* **153** 179
[44] Zhou Q H, Zha S, Liu P G, Liu C X, Bian L A, Zhang J H, Liu H Q and Ding L 2018 *Materials* **11** 2409
[45] Xiong H, Ji Q, Bashir T and Yang F 2020 *Opt. Express* **28** 13884
[46] Gao F, Zhu Z H, Xu W, Zhang J F, Guo C C, Liu K, Yuan X D and Qin S Q 2017 *Opt. Express* **25** 9579
[47] Zhang Y, Li Y, Cao Y, Liu Y and Zhang H 2017 *Opt. Commun.* **382** 281
[48] Yang J W, Zhu Z H, Zhang J F, Guo C C, Xu W, Liu K, Yuan X D and Qin S Q 2018 *Sci. Rep.* **8** 3239
[49] Qi L M and Liu C 2019 *Opt. Mater. Express* **9** 1298
[50] Nejat M and Nozhat N 2019 *IEEE Trans. Nanotech.* **18** 684
[51] Hanson G W 2008 *J. Appl. Phys.* **103** 064302
[52] Fang Z, Wang Y, Schlather A E, Liu Z, Ajayan P M, García de Abajo F J, Nordlander P, Zhu X and Halas N J 2014 *Nano Lett.* **14** 299
[53] Smith D R, Vier D C, Koschny T and Soukoulis C M 2005 *Phys. Rev. E* **71** 036617
[54] Li J S, Yan D X and Sun J Z 2019 *Opt. Mater. Express* **9** 2067
[55] Wang B X, Wang G Z and Wang L L 2016 *Plasmonics* **11** 523
[56] Hu N, Wu F L, Bian L A, Liu H Q and Liu P G 2018 *Opt. Mater. Express* **8** 3899
[57] Xiao D Y, Zhu M M, Sun L M, Zhao C, Wang Y R, Teo E H T, Hu F J and Tu L C 2019 *ACS Appl. Mater. Inter.* **11** 43671
[58] Ma W, Chen H, Hou S, Huang Z, Huang Y, Xu S, Fan F and Chen Y 2019 *ACS Appl. Mater. Inter.* **11** 25369